fire

MDPI

Article

Effects of Nano-Nickel Oxide on Thermokinetics, Thermal Safety, and Gas-Generating Characteristics of 5-Aminotetrazole Thermal Degradation

Dan Zhang, Lifeng Xie and Bin Li *

School of Chemistry and Chemical Engineering, Nanjing University of Science and Technology, Nanjing 210094, China
* Correspondence: libin@njust.edu.cn

Abstract: 5-aminotetrazole (5AT) has been widely used as a fuel in SPGGs for its high nitrogen content, heat resistance, and environmentally friendly product. However, 5AT-based propellants still have disadvantages, such as a high exhaust temperature and unstable combustion rate, which somewhat limit their application. Given that transition metal oxides are typically employed in small quantities to enhance the performance of solid propellants, this study selected nickel oxide (NiO) nanoparticles as a catalyst and employed them in conjunction with 5AT via mechanical ball milling to investigate their impact on the pyrolysis behavior of 5AT. It was found that the nanoscale NiO particles can significantly reduce the thermal degradation temperature of 5AT according to TG-DSC tests. The calculation of the energy required to initiate the pyrolysis of 5AT using three kinetic methods, namely Friedman (FR), Flynn–Wall–Ozawa (FWO), and Kissinger–Akahira–Sunose (KAS), indicated that the use of NiO nanoparticles can reduce the energy required by more than 46 kJ mol^{-1}, thereby increasing the likelihood of 5AT pyrolysis. Meanwhile, the reduced thermal safety parameters indicated that NiO makes 5AT more susceptible to thermal decomposition due to thermal explosion transition, so more care is needed for the storage of 5AT. Moreover, the TG-FTIR test was conducted to study the pyrolysis mechanism with or without NiO; the results showed that NiO exerts different catalytic effects on the gas products. The results from this study can offer direction and recommendations for future research on solid propellants.

Keywords: nano-NiO; 5-amino-1H-tetrazole; catalyst; degradation mechanism; kinetic; safety parameters

Citation: Zhang, D.; Xie, L.; Li, B. Effects of Nano-Nickel Oxide on Thermokinetics, Thermal Safety, and Gas-Generating Characteristics of 5-Aminotetrazole Thermal Degradation. *Fire* **2023**, *6*, 172. https://doi.org/10.3390/fire6040172

Academic Editors: Yongzheng Yao, Jinlong Zhao, Qiang Wang and Zihe Gao

Received: 24 March 2023
Revised: 19 April 2023
Accepted: 20 April 2023
Published: 21 April 2023

1. Introduction

Solid propellant gas generators (SPGGs) are an emerging technology in the field of Halon alternative research, which has potential applications for fire suppression in dry bays and nacelles [1,2]. Fire suppression agents can be expelled under the reaction of solid propellant, including 1,1,1,2,3,3,3-heptafluoropropane, pentafluoroethane, or potassium carbonate. SPGGs have some exceptional properties, which include easy storage, rich in inert gases, and no liquid component, all of which significantly enhance its applicability in aviation firefighting.

According to the Next Generation Fire Suppression Technology Program [3], green energetic materials (GEMs) are widely used as fuels in SPGGs. Examples of GEMs include 5-aminotetrazole (5AT), bitetrazole (BT), guanidinium bitetrazole (GBT), triaminoguanidinim nitrate (TAGN), and bis(aminotetrazolyl)tetrazine (BTATZ). Among the studied fuels, 5AT (as shown in Figure 1) is the most readily available, and its commercial application prospect is the broadest. In contrast, many of the other fuels considered have limited commercial availability. As an environmentally friendly green energetic material, 5-amino-1h-tetrazole (5AT/CH_3N_5) has become the top candidate for use in solid propellants, rocket engines, airbags, and fire extinguishing areas. What makes 5AT extremely attractive is its surprisingly potential energy properties, e.g., high nitrogen content (82.3%), high formation

enthalpy (208.7 kJ mol^{-1}), moderate mechanical, and thermal sensitivity. Once the mixtures of 5AT and oxidizers (strontium nitrate, potassium nitrate, etc.) are ignited, violent redox reactions will immediately take place with the generation of large amounts of gases and heat, creating desirable impetus. Undoubtedly, the pyrolysis behavior of thermal hazard substances usually plays a crucial role in burning rates and gas production performance for propellants, pyrotechnics, and explosives. Pyrolysis of 5AT is also regarded as the fundamental step to generate gaseous products which support fuel ignition, burning, and energy release. To elucidate the mechanism governing propulsive performance, it appears essential to analyze the thermal degradation behavior of 5AT.

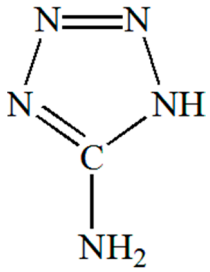

Figure 1. The chemical structure of 5-aminotetrazole.

Pyrolysis analysis is an effective method to study the properties of energetic materials, which is a crucial chemical conversion method that can help us to understand the thermal and combustion behaviors. Thermogravimetry (TG) technology can exhibit the generation of products in different phases in a given temperature range and the kinetic parameters can be obtained through the TG data, which is of great importance for the prediction and understanding of the pyrolysis and combustion characteristics of energetic materials and can further expand its application ranges. Thermogravimetry combined with Fourier transform infrared spectroscopy (TG-FTIR) is another method to investigate these properties, which can convert the inherent energy inside the molecule of energetic materials to the solid, gas and liquid products, which allow us determine the decomposition pathways of the energetic materials and aid their application, management, and computer simulations.

However, 5AT-based propellants have some limitations in their combustion and thermal decomposition behaviors that hinder their development [4,5]. These include the high exhaust temperature and the unstable burning rate. To improve its combustion performance, different chemical compounds have been incorporated into 5AT-based propellants [6,7]. Research has indicated that transition metal oxides (TMOs) can be employed in minute quantities in solid propellants to enhance their combustion characteristics. Examples of these TMOs include Fe_2O_3, ZnO, CuO, NiO, and TiO_2. The pyrolysis property of combustible materials is a fundamental aspect of material combustion [8]. Therefore, the thermal stability of catalyzed 5AT is essential for its safe handling, storage, and usage. Thus, to study the pyrolysis process and thermal behavior of 5AT with the addition of additives is necessary for its practical application. The objective of this study is to examine how nano-sized NiO affects the thermal decomposition characteristics of 5AT.

In previous studies, the effects of TMO addition have been conducted on traditional propellant ingredients [9,10]. Prajakta et al. [9] and Wang et al. [10] conducted studies on the effect of two different catalytic agents containing nano-copper oxide and nano-sized NiO on the degradation behavior of AP-based propellants, respectively. Prajakta et al. [9] found that the degradation temperature and the activation energy decreased with the addition of nano-copper oxide. Wang et al. [10] proposed that the degradation temperature of AP decreased by 93 °C after adding 2% nano-sized NiO. Paletsky et al. [11] studied the degradation kinetic characteristics of 5AT at high heating rates (~100 °C s^{-1}), and distinguished two routes of 5AT decomposition. Levchik et al. studied the energies of atomic bonding of 5AT tautomers during its decomposition process [12]. A review of the

literature reveals that the kinetic parameters, thermodynamic parameters, and thermal safety parameters of 5AT with catalysts have not been extensively studied.

This article presents a comprehensive analysis of the thermostability of pure 5AT and its mixture with nano-sized NiO. The study used thermogravimetry (TG), differential scanning calorimetry (DSC), and Fourier transform infrared (FTIR) spectroscopy to evaluate the thermal kinetics, thermodynamic parameters, and thermal safety. The dynamic thermal TG-DSC techniques were used to obtain the mass and heat flow variations with the increase in temperature. The weight-loss curves were used to evaluate the thermal kinetics and thermodynamic parameters, while the heat flow curves were used to evaluate the thermal safety. The 3D spectrogram was plotted using FTIR analysis to identify the evolved gas distribution during pyrolysis. In this study, NiO nanoparticles were investigated due to their catalytic effects on the degradation process of 5AT. This may have implications for the research field of solid propellant gas generators in the aviation industry.

2. Theoretical Considerations

An examination of the degradation kinetics and pyrolysis mechanism of 5AT was conducted using three iso-conversional methods (FWO, FR, and KAS). These approaches can estimate the activation energy as an outcome of the conversion process without assuming any decomposition model. This is provided that at least three different heating rates are used. Below are the detailed descriptions of each method. A general expression for degradation kinetics can be found in equation [13].

$$\beta \frac{d\alpha}{dT} = Af(\alpha)exp\left(-\frac{E}{RT}\right) \tag{1}$$

where α, T, and β denote the conversion rate, temperature, and heating rate constant ($\beta = \frac{dT}{dt} = Constant$), respectively. A, E, and $f(\alpha)$ are the kinetic triplets, which refer to the pre-exponential factor, the activation energy, and the kinetic function, respectively. R is the gas constant (8.314 J mol^{-1} K^{-1}). In terms of weight loss, the conversion coefficient α is calculated as follows [14]:

$$\alpha = \frac{W_0 - W_t}{W_0 - W_f} \tag{2}$$

Here, the instant mass of a sample at time t, W_t, represents the difference between its initial weight, W_0, and its final weight, W_f, which is the weight of the sample after it has been completely decomposed.

2.1. FR Method [15]

As a result of Friedman's method, activation energy is determined by TG data for different heating rates, and the mathematical equation may be expressed as follows:

$$\ln\frac{d\alpha}{dt} = \ln[Af(\alpha)] - \frac{E}{RT} \tag{3}$$

By mathematically plotting $\ln(d\alpha/dt)$ vs. $1/T$, a linear relation indicating a slope equal to $-E/R$ can be obtained.

2.2. FWO Method [16]

In terms of the FWO method, it is an integral approach that does not depend on the degradation mechanism. It can be expressed in logarithmic form as follows:

$$\lg\beta = \ln\frac{AE}{Rg(\alpha)} - 2.315 - 0.4567\frac{E}{RT} \tag{4}$$

An estimate of E can be obtained by linear regression of $\ln\beta$ vs. $1/T$ at a fixed conversion with a slope of $0.4567E/RT$.

2.3. KAS Method [17]

The KAS method, similar to the FWO method, is an integral method. The following is the equation for KAS:

$$\ln\frac{\beta}{T^2} = \ln\frac{AR}{Eg(\alpha)} - \frac{E}{RT} \quad (5)$$

Plotting $\ln(\beta/T^2)$ vs. $1/T$ allows the calculation of E for each degree of conversion values.

3. Experimental Setup

3.1. Sample Preparation

The 5AT base (Table 1 presents the materials information) was blended with 2% nano-sized NiO particles. As a solvent, alcohol was used to ensure a uniform dispersion at a volume ratio of 1:3 for both pure 5AT and 5AT–NiO mixtures. It can prevent a reaction from occurring between 5AT and NiO. On the other hand, anhydrous ethanol, as a fluid, in the ball milling process, it allows 5AT and NiO to be fully dispersed and flowing, and it is beneficial to achieve a homogeneous blend between 5AT and NiO. The mixtures were then ground using SFM-2 planetary centrifugal mill at 150 rpm for 24 h. To remove the solvent, the powders were dried in a vacuum oven for eight hours. A total of two samples were prepared: a pure 5AT foundation material (designated 5AT–1) and a pure 5AT foundation material containing 2% nano-sized NiO (designated 5AT–2).

Table 1. Information on the ingredients of propellant samples.

Constituents	Purity	Particle Size	Source	Type
5AT	≥99.0%	5~20 μm	Dongyang Tianyu Chemical Co., Ltd, in Dongyang, China.	Base
Nano-sized NiO	≥99.8%	<50 nm	Sigma-Aldrich Corporation, in Shanghai, China.	Additive

3.2. Thermal Decomposition Measurement

An analysis of the thermal properties was carried out using TG and TG-DSC at temperatures ranging from room temperature to 800 °C. To obtain the thermal decomposition parameters for comparison, conventional TG measurements with four different heating rates of 5, 10, 15, and 20 °C min^{-1} were conducted. For each experimental run, approximately 3 mg of the powdery sample was evenly spread in an open alumina cup. In the course of the process, the nitrogen purge flow was maintained at 100 mL min^{-1}.

3.3. FTIR Test

To differentiate the evolved gas from the propellant, a Fourier transform infrared (FTIR) spectrometer in conjunction with a thermobalance was employed to analyze the degradation behaviors of the 5AT samples. The FTIR and the TG analyzer were connected by a transfer line. The pure helium purge flow was set at 100 mL min^{-1} during the test.

4. Results and Discussion

4.1. Thermal Degradation Behavior

TG and DTG profiles for 5AT–1 and 5AT–2 with a characteristic heating rate are shown in Figures 2 and 3. Table 2 lists the characteristic temperatures of different mass-loss stages at different conversion rates. Comparing Figure 2 with Figure 3, the trends of the mass loss curves were similar, while both the degradation of 5AT–1 and 5AT–2 exhibited four degradation stages, which can be seen from the four peaks in DTG. The pyrolysis process is attributed to the decomposition of crystalline water inside the 5AT molecular structure when the temperature is below 100 °C.

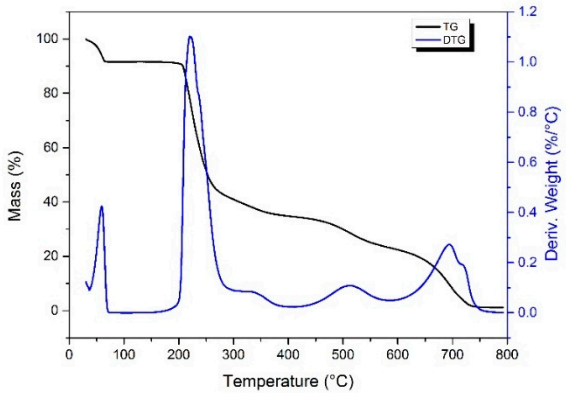

Figure 2. The TG-DTG curves of 5AT–1 at 10 °C min^{-1}.

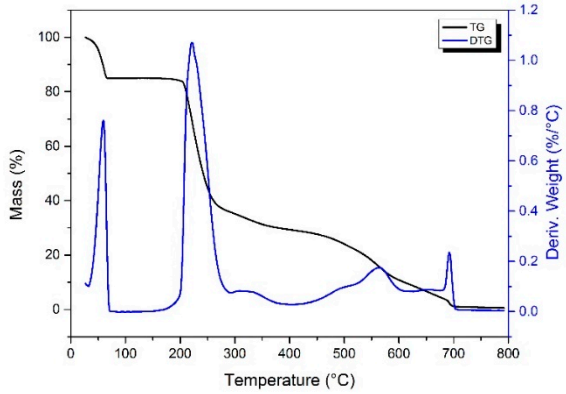

Figure 3. The TG-DTG curves of 5AT–2 at 10 °C min^{-1}.

Table 2. Characteristic temperatures at different conversions of mass-loss stages.

Sample	β °C min^{-1}	0.1	0.2	0.3	0.4	0.5	0.6	0.7	0.8	0.9
5AT–1	5	209.6	216.7	224.4	234.6	254.2	342.0	502.4	612.3	669.3
	10	215.9	224.1	233.1	243.9	261.7	343.1	516.0	644.0	692.2
	15	220.7	230.8	240.8	252.4	271.7	358.6	530.0	656.8	701.7
5AT–2	5	208.5	214.4	220.9	228.7	240.2	294.6	458.1	530.8	578.5
	10	214.7	222.7	230.9	240.5	253.7	310.3	479.5	553.8	622.0
	15	219.9	229.3	238.4	248.9	264.1	332.1	495.9	548.7	579.1

However, from Table 2, it can be found that the characteristic temperatures at different conversions for 5AT–1 were obviously lower than those for 5AT–2, indicating that nano-sized NiO particles could reduce the decomposition temperature. This result implies that the thermostability of 5AT–2 has been slightly reduced with NiO addition, even though a similar decomposition process occurs.

4.2. Reaction Kinetics of Isoconversions

To calculate the activation energy, three heating rates and three iso-conversional kinetic methods (FR, FWO, and KAS approaches) were employed to analyze the thermal degradation characteristics. According to Equations (3)–(5), the linear regression parameters against $1/T$ can be calculated, respectively using the three thermal kinetic methods (FR, FWO, and KAS). The activation energy for each conversion was calculated based on the linear relationship between variables. Table 3 shows the activation energy results and the linear correlation coefficients for 5AT degradation.

Table 3. Characteristic kinetic parameters for 5AT–1 and 5-AT-2, varying with conversion method.

Sample	α	FR		FWO		KAS	
		E/kJ mol^{-1}	R^2	E/kJ mol^{-1}	R^2	E/kJ mol^{-1}	R^2
5AT–1	0.1	98.75	0.84	188.60	1.00	190.22	0.99
	0.2	116.65	0.97	151.40	0.99	150.96	0.99
	0.3	122.11	0.99	135.96	0.99	134.56	0.99
	0.4	119.18	0.99	130.99	0.99	129.16	0.99
	0.5	180.68	0.87	140.47	0.95	138.80	0.94
	0.6	144.44	0.47	203.07	0.97	147.81	0.64
	0.7	187.53	0.99	196.14	0.98	193.13	18.30
	0.8	187.01	0.97	156.69	0.99	149.70	0.99
	0.9	293.53	0.99	240.70	0.99	237.20	0.99
	Mean	161.10	0.90	171.56	0.98	163.51	2.87
5AT–2	0.1	98.04	1.00	182.32	0.99	183.61	0.99
	0.2	112.97	0.98	143.62	0.99	142.81	0.99
	0.3	93.81	1.00	125.85	1.00	123.99	1.00
	0.4	89.97	1.00	113.57	1.00	110.92	1.00
	0.5	74.85	0.96	100.56	1.00	97.02	1.00
	0.6	63.26	0.98	78.14	0.95	72.41	0.93
	0.7	207.34	0.98	130.03	1.00	124.28	1.00
	0.8	213.13	0.46	201.49	0.70	198.33	0.67
	0.9	81.82	0.11	21.75	0.03	8.35	0.03
	Mean	115.02	0.83	121.92	0.85	117.97	0.84

From Table 3, it can be seen that the square of the correlation coefficient at higher conversions were much smaller than 1 when the kinetic calculations were performed on the sample doped with nano-sized NiO, which may be responsible for the pyrolysis process being dominated by the reaction temperature at the beginning of the pyrolysis reaction. As the reaction continues, the catalytic effect of NiO plays an important role in the later pyrolysis process, which promotes the pyrolysis reaction and more gas products are rapidly generated; this causes the instability of the pyrolysis process in the later stage with an increased conversion rate. Therefore, the square of the correlation coefficient at higher conversions were much smaller due to the catalytic effect of NiO and the accelerated generation of gas products.

The mean value of E for 5AT–1 was 161.1–171.6 kJ mol^{-1}, while that for 5AT–2 was 115.0–121.9 kJ mol^{-1} (varying with the kinetic methods). The derived E of 5AT–2 was much lower than that of 5AT–1, indicating that the nano-sized NiO significantly affected 5AT activity. As a result, the 5AT decomposition with NiO required a lower temperature and less energy.

The correlation relationships between the activation energy (E) obtained from the three kinetic methods (FR, FWO, and KAS methods) and the conversion (α) are shown in Figures 4–6. Generally speaking, the activation energy values of 5AT–2 were mostly lower than those of 5AT–1 in the conversion (α) range from 0.1 to 0.9. Kinetic parameters are influenced by multiple factors, such as reaction time, temperature, reaction rate, conversion, etc. Moreover, the kinetic parameters also can be influenced by each other. As the thermal decomposition reaction progresses, the reaction time, temperature, and conversion are increasing, but the reaction rate is not a constant and it causes the activation energy and conversion rate to keep fluctuating, which further affects the instability of reaction.

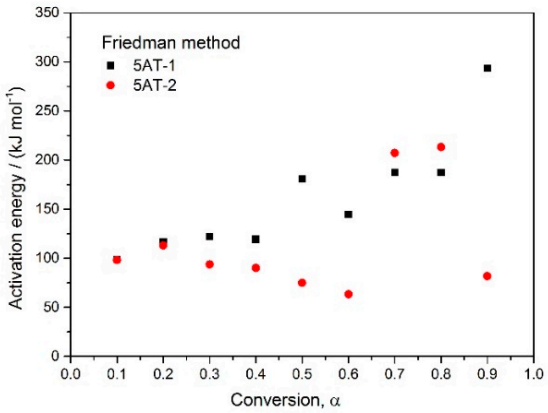

Figure 4. Comparison for E vs. α between 5AT–1 and 5AT–2 obtained using FR method.

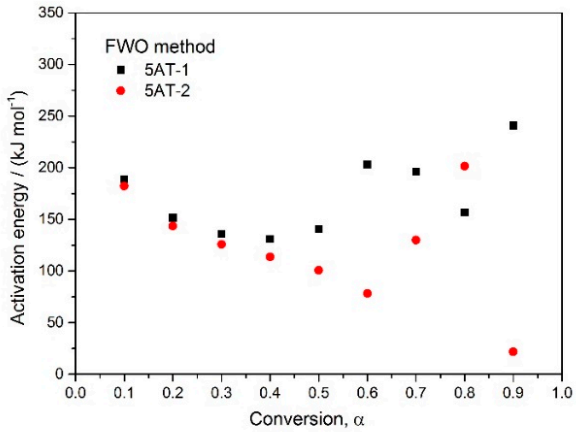

Figure 5. Comparison for E vs. α between 5AT–1 and 5AT–2 obtained using FWO method.

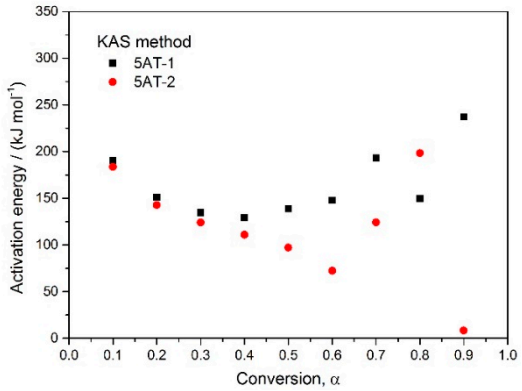

Figure 6. Comparison for E vs. α between 5AT–1 and 5AT–2 obtained using KAS method.

The differences between the FR, KAS, and FWO methods, according to the results in Figures 4–6, may be attributed to the formula's calculation principle. Specifically, the independent variables are all associated with temperature (1/T), but the dependent variables are different for these three methods. For the FR method, the dependent variable ($\ln(d\alpha/dt)$) is related to time (t) and conversion (α), which is only directly influenced by the accuracy of the experimental recordings of time (t) and conversion (α) accompanied by no approximations for the formulation's reasoning and expression. For the KAS and FWO methods, both the formulations' reasoning processes and expressions are adjusted by several approximations. Therefore, there is a difference between these three methods due to the formula's calculation principle and reasoning process. However, no matter what

method is used, the mean activation energy calculation results had similar variation trends and effectively reflected the catalytic effect of NiO.

4.3. Effects of Heating Rate on DSC Curves

Figures 7 and 8 show the DSC curves of 5AT–1 and 5AT–2 at 150–400 °C using four different heating rates. The decomposition temperature of both 5AT–1 and 5AT–2 was shifted to higher temperatures.

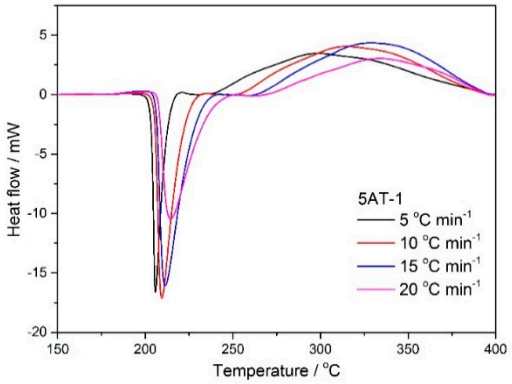

Figure 7. DSC profiles of 5AT–1 using four different heating rates.

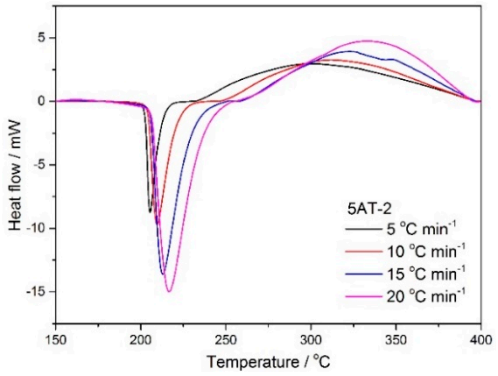

Figure 8. DSC profiles of 5AT–2 using four different heating rates.

Three characteristic temperatures were obtained from the DSC profiles, i.e., T_0, T_{onset}, and T_p; the determination method was same as that used in previous studies [18]. Figure 9 shows the characteristics of the temperature changes (T_o, T_{onset}, and T_p). With the growth of the heating rate, the characteristic temperatures increased. On the other hand, the T_o, T_{onset}, and T_p of 5AT–2 were lower than those of 5AT–1.

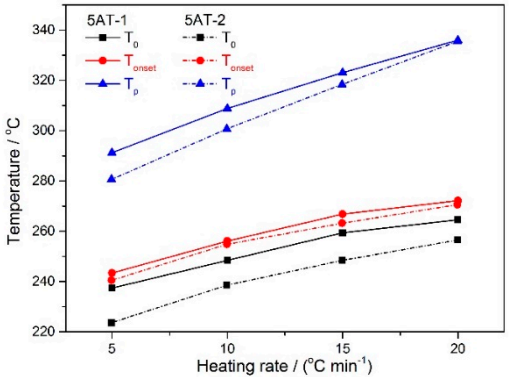

Figure 9. The effect of varying the heating rate of 5AT–1 and 5AT–2 on T_o, T_{onset}, and T_p.

4.4. Kinetic Parameters Derived from DSC Curves

The thermal decomposition of the two 5AT samples was investigated using the ASTM method E698 [19] to determine the Arrhenius parameters. To obtain the parameter value of A, the decomposition was deemed to follow the first-order kinetics. As a result, the first-order kinetics model fit the overall observed decomposition behavior of both 5AT samples over this temperature range, as evidenced using the linear regression method. The linear representation of $\ln(\beta/T_p{}^2)$ vs. $1/T_p$ made it possible to determine E from the linear slope, as shown in Figure 10. The logarithm of A, lg$A$, can be derived from the numerical relationship from ASTM E698:

$$A = \beta\left(\frac{E}{RT_p{}^2}\right)exp\left(\frac{E}{RT_p}\right) \tag{6}$$

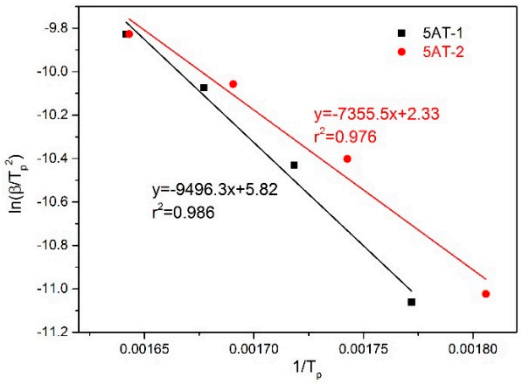

Figure 10. The numerical relationship between $\ln(\beta/T_p{}^2)$ and $1/T_p$ for 5AT–1 and 5AT–2.

As for the thermodynamic parameters of the activation reaction, the thermal kinetic parameters were also investigated. Shown in Equations (7)–(11), $\Delta G^{\neq}$, $\Delta H^{\neq}$, and $\Delta S^{\neq}$ are free energy, enthalpy, and entropy of the activation, respectively.

$$Aexp(-E/RT) = \frac{k_B T}{h}exp\left(-\Delta G^{\neq}/RT\right) \tag{7}$$

$$-\Delta H^{\neq} = E - RT \tag{8}$$

$$\Delta G^{\neq} = \Delta H^{\neq} - T\Delta S^{\neq} \tag{9}$$

A summary of the characteristic kinetic parameters is presented in Table 4. Compared to 5AT–1, 5AT–2 remained lower in activation energy. The positive values of $\Delta G^{\neq}$ imply that the propellants require heating to undergo exothermic decomposition. Moreover, the higher thermodynamic value of 5AT–1 indicates a higher heat demand for exothermic decomposition.

Table 4. Characteristic kinetic parameters calculated using ASTM methods.

Sample	E_a (kJ/mol)	lg$A$ (s^{-1})	r^2	$\Delta G^{\neq}$ (kJ/mol)	$\Delta H^{\neq}$ (kJ/mol)	$\Delta S^{\neq}$ (kJ/mol)
5AT–1	78.95	6.50	0.99	94.10	74.11	−34.35
5AT–2	61.15	4.88	0.98	80.03	56.38	−41.21

4.5. Thermal Safety Studies

When the heating rate approaches zero, i.e., $\beta \to 0$, the values of T_{00}, T_{e0}, and T_{p0} can be calculated using Equation (10). Equation (11) [18] can be used to estimate the temperature of self-accelerating decomposition.

$$T_{0(or\ e\ or\ p)} = T_{00(or\ e0\ or\ p0)} + b\beta + c\beta^2 + d\beta^3 + e\beta^4 \quad (10)$$

where b, c, d, and e are coefficients.

$$T_{SADT} = T_{e0} \quad (11)$$

In Equation (12), T_{TIT} is the thermal ignition temperature [20]. Alternatively, the thermal explosion critical temperature (T_b) can be determined by incorporating E and T_{p0} into the equation below.

$$T_{TIT(or\ b)} = \frac{E - \sqrt{E^2 - 4ERT_{eo(orp0)}}}{2R} \quad (12)$$

All the thermal safety values of the propellants are listed in Table 5. We can see that both T_{SADT} and T_{TIT} of 5AT–1 were higher than those of 5AT–2, indicating that the NiO addition into 5AT resulted in a reduced resistance to heat and thermal safety of the 5AT propellant. Meanwhile, the critical value of T_b for 5AT–2 was lower than that of 5AT–1, indicating that the process of thermal explosion for 5AT–2 occurred more readily.

Table 5. The derivative parameters of 5-AT-1 and 5AT–2 samples.

Sample	5AT–1	5AT–2
T_{00} (°C)	229.3	214.7
$T_{SADT/e0}$ (°C)	235.4	232.6
T_{p0} (°C)	277.6	263.2
T_{TIT} (°C)	241.5	240.9
T_b (°C)	286.2	273.4

4.6. Gas Product Analysis Using Fourier Transform Infrared Spectroscopy

Following the acquisition of all FTIR data, a typical 2D spectrogram for the two samples were plotted from the TG-FTIR. The temperature and wavenumber of 5AT–1 and 5AT–2 were used to identify the related evolved gas information. By comparing the two spectrograms, it was observed that the addition of nano-sized NiO generated new gases.

As can be seen in Figures 11 and 12, two spectrum band peaks within 3400–3250 cm^{-1} suggest that there were symmetrical stretching vibrations of primary amine (–NH_2) groups within the organic compounds. The absorption bands at 1650–1500 and 3336 cm^{-1} could be attributed to the in-plane bending vibrations and stretching vibrations of secondary amine (–NH) groups. The presence of the absorption band at 2150–2000 cm^{-1} was considered to indicate the existence of hydrazoic acid (HN_3). Additionally, another remarkable spectrum band at 2410–2200 cm^{-1} was associated with the formation of a cyanogroup (–CN).

NiO exerts different catalytic effects on different groups. For the –NH and –CN groups, the initial evolving temperature is moved forward with the addition of NiO, and the evolving temperature range of HN_3 is extended due to the presence of NiO. However, the terminal temperature of –NH_2 is shortened when adding NiO.

Previous research had confirmed that the generation of CH_2N_2 can be detected at 250~500 °C during the pyrolysis process. Therefore, the –NH group is associated with the generation of CH_2N_2. The gas product of NH_2CN can be detected when the temperature is over 500 °C. The –CN is most likely to belong to the characteristic group of NH_2CN. The two spectrum band peaks within the 3400–3250 cm^{-1} range are the characteristic absorption peaks of HCN.

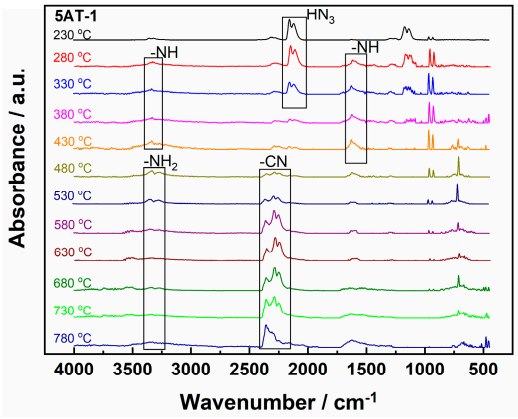

Figure 11. The IR spectrum of 5AT–1.

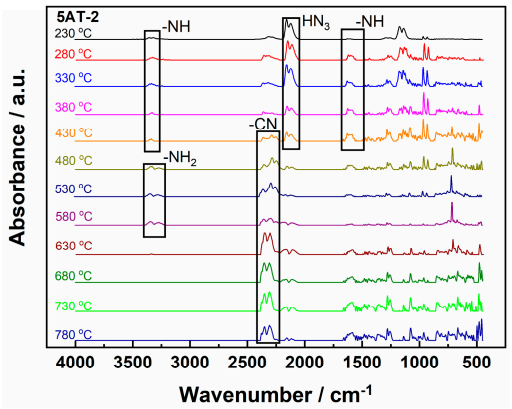

Figure 12. The IR spectrum of 5AT–2.

Based on the above analysis, there were no new gas products generated when adding nano-sized NiO, but different catalytic effects on different groups were obvious. Specifically, the initial evolving temperature of CH_2N_2 was detected in advance (about 50 °C earlier) with the presence of NiO. Moreover, the generation of HCN followed a similar variation trend. The evolving temperature range of HN3 was extended from 330 °C to 430 °C with the same initial temperature. In particular, the temperature range of NH_2CN was shortened from 780 °C to 580 °C under the same terminal temperature.

5. Conclusions

The addition of nano-sized NiO lowered the characteristic temperature values at different conversions, as shown by the comparison of the TG-DTG curves. The iso-conversional reaction kinetics indicated that the nano-sized NiO has a significant catalytic effect on the 5AT decomposition process by reducing the activation energy and facilitating the reaction process. The thermodynamic parameters derived from the DSC study, including the free energy, entropy, and enthalpy of activation, indicated that less heat is required for the exothermic decomposition to occur when NiO is present, further corroborating the catalytic activity of NiO. From the thermal safety studies, it was more likely to transform from degradation to explosion for 5AT with the addition of NiO. The 5AT catalyzed by nano-sized NiO was more heat sensitive during storage than raw 5AT. Moreover, the TG-FTIR test was conducted to study the pyrolysis mechanism with or without NiO; the results showed that NiO exerts different catalytic effects on the gas products. In a future simulation study, the kinetic parameters, thermodynamic parameters, and evolved gases obtained in this study will be incorporated into the degradation model for propellants.

Author Contributions: Writing—original draft preparation, D.Z.; investigation and data curation, L.X.; writing—review and editing, B.L. All authors have read and agreed to the published version of the manuscript.

Funding: This research received no external funding.

Conflicts of Interest: The authors declare no conflict of interest.

References

1. Yoon, S.S.; Kim, H.Y.; Hewson, J.C.; Suo-Anttila, J.M.; Glaze, D.J.; Desjardin, P.E. A Modeling Investigation of Suppressant Distribution from a Prototype Solid-Propellant Gas-generator Suppression System into a Simulated Aircraft Cargo Bay. *Dry. Technol.* **2007**, *25*, 1011–1023. [CrossRef]
2. Fallis, S.; Reed, R.; Lu, Y.C. Advanced Propellant/Additive Development for Fire Suppressing Gas Generators. *Halon Opt. Tech. Work. Conf.* **2000**, 361–370. Available online: https://tsapps.nist.gov/publication/get_pdf.cfm?pub_id=909449 (accessed on 1 January 2001.).
3. Neidert, J.B.; Black, R.E.; Lynch, R.D.; Martin, J.D.; Simpson, T. Fighting Fire with Fire: Solid propellant Gas Generator Technology for Fire Suppression. *JANNM Propuls. Conf.* **1998**, *11*, 77–86.
4. Zhang, D.; Lu, S.; Gong, L.L.; Cao, C.Y.; Zhang, H.P. Effects of calcium carbonate on thermal characteristics, reaction kinetics and combustion behaviors of 5AT/Sr $(NO_3)_2$ propellant. *Energy Convers. Manag.* **2016**, *109*, 94–102. [CrossRef]
5. Zhang, D.; Lu, S.; Zhang, H. Exploring mechanisms of particle size effects of iron oxide on thermal behaviors and combustion characteristics for 5AT/Sr$(NO_3)_2$ Propellant. In Proceedings of the 46th AIAA Thermophysics Conference, Washington, DC, USA, 13–17 June 2016.
6. Degirmenci, E. Effects of grain size and temperature of double base solid propellants on internal ballistics performance. *Fuel* **2015**, *146*, 95–102. [CrossRef]
7. Jawalkar, S.; Kurva, R.; Sundaramoorthy, N.; Dombe, G.; Singh, P.P.; Bhattacharya, B. Studies on high burning rate composite propellant formulations using TATB as pressure index suppressant. *Central Eur. J. Energetic Mater.* **2012**, *9*, 237–249.
8. Jiang, L.; Xiao, H.-H.; He, J.-J.; Sun, Q.; Gong, L.; Sun, J.-H. Application of genetic algorithm to pyrolysis of typical polymers. *Fuel Process. Technol.* **2015**, *138*, 48–55. [CrossRef]
9. Patil, P.R.; Krishnamurthy, V.N.; Joshi, S.S. Effect of nano-copper oxide and copper chromite on the thermal decomposition of ammonium perchlorate. *Propellants Explos. Pyrotech.* **2008**, *33*, 266–270. [CrossRef]
10. Wang, Y.; Zhu, J.; Yang, X.; Lu, L.; Wang, X. Preparation of NiO nanoparticles and their catalytic activity in the thermal decomposition of ammonium perchlorate. *Thermochim. Acta* **2005**, *437*, 106–109. [CrossRef]
11. Paletsky, A.A.; Budachev, N.V.; Korobeinichev, O.P. Mechanism and kinetics of the thermal decomposition of 5-aminotetrazole. *Kinet. Catal.* **2009**, *50*, 627–635. [CrossRef]
12. Levchik, S.V.; Ivashkevich, O.A.; Balabanovich, A.I.; Lesnikovich, A.I.; Gaponik, P.N.; Costa, L. Thermal decomposition of aminotetrazoles: Part 1. 5-Aminotetrazole. *Thermochim. Acta* **1992**, *207*, 115–130. [CrossRef]
13. Rocco, J.A.F.F.; Lima, J.E.S.; Frutuoso, A.G.; Iha, K.; Ionashiro, M.; Matos, J.R.; Suárez-Iha, M.E.V. Thermal degradation of a composite solid propellant examined by DSC. *J. Therm. Anal. Calorim.* **2004**, *75*, 551–557. [CrossRef]
14. Ozawa, T. Kinetic analysis of derivative curves in thermal analysis. *J. Therm. Anal. Calorim.* **1970**, *2*, 301–324. [CrossRef]
15. Chrissafis, K. Kinetics of thermal degradation of polymers: Complementary use of isoconversional and model-fitting methods. *J. Thermal Anal. Calorim.* **2008**, *95*, 273–283. [CrossRef]
16. Budrugeac, P.; Homentcovschi, D.; Segal, E. Critical analysis of the isoconversional methods for evaluating the activation energy. I. Theoretical background. *J. Thermal Anal. Calorim.* **2000**, *63*, 457–463. [CrossRef]
17. Leszczynska, A.; Pielichowski, K. Application of thermal analysis methods for characterization of polymer/montmorillonite nanocomposites. *J. Thermal Anal. Calorim.* **2008**, *93*, 677–687. [CrossRef]
18. Hu, R.Z.; Gao, S.L.; Zhao, F.Q.; Shi, Q.Z.; Zhang, T.L.; Zhang, J.J. *Thermal Analysis Kinetics*, 2nd ed.; Science Press: Beijing, China, 2008.
19. *ASTM E 698-05*; Standard Test Methods for Arrhenius Kinetic Constants for Thermally Unstable Materials Using Differential Scanning Calorimetry and the Flynn/Wall/Ozawa Method. American Society for Testing and Materials: West Conshohocken, PN, USA, 1979.
20. Zhang, T.L.; Hu, R.Z.; Xie, Y.; Li, F.P. The estimation of the critical temperature of thermal explosion for energetic materials using non-isothermal DSC. *Thermochim. Acta* **1994**, *244*, 171–176.